1-1-2011

Enhancement of the capacitance in TiO2 nanotubes through controlled introduction of oxygen vacancies

Maryam Salari
msalari@uow.edu.au

Konstantin K. Konstantinov
University of Wollongong, konstan@uow.edu.au

Hua-Kun Liu
University of Wollongong, hua@uow.edu.au

Journal of Materials Chemistry

Cite this: *J. Mater. Chem.*, 2011, **21**, 5128

www.rsc.org/materials

PAPER

Enhancement of the capacitance in TiO_2 nanotubes through controlled introduction of oxygen vacancies

Maryam Salari,* Konstantin Konstantinov and Hua Kun Liu

Received 25th November 2010, Accepted 2nd February 2011
DOI: 10.1039/c0jm04085a

The many applications of high energy storage devices have forged an increasing interest in research areas related to electrochemical capacitors. Here, in this work, we present a facile method for the fabrication of self-organized titania nanotubes grown by anodic oxidation of titanium foil with different subsequent heat-treatment regimes for use as binder-free working electrodes in supercapacitor applications. The capacitance of these highly ordered titania nanotubes, when exposed to a reductive atmosphere during annealing, was determined to be well above 900 μF cm^{-2}, confirming that the capacitance contribution was pseudocapacitive in nature. The behaviour of oxygen depleted titania in the anatase to rutile (A → R) phase transformation and also in electrochemical charge storage has been studied in detail. It was found that upon the reduction of Ti^{4+} to Ti^{3+}, with oxygen depletion of the structure, the A → R phase transformation was promoted. In addition, the fabricated electrodes showed highly reversible charge–discharge stability.

Introduction

Supercapacitors are being increasingly investigated as a viable charge storage technology. They are classified into three general groups based on their charging mechanism: non-faradic supercapacitors (electric double layer capacitors (ELDCs)),[1] faradic supercapacitors (pseudocapacitors),[1,2] and hybrid supercapacitors.[3] So far, different types of carbon, such as carbon nanotubes, carbon aerogels, and activated carbon,[4–6] as well as transition metals, such as Ru,[1,2] Ni,[6] Mn,[1] and their oxides, have been employed as active materials in the fabrication of supercapacitor electrodes. Over the last decade, titania (TiO_2) has been investigated for use as a supercapacitor electrode material due to its semiconducting properties and chemical stability.[7–17] It is well-known that high surface area,[2] high conductivity,[6,18] and interconnectivity of the active material will strongly enhance the capacitance properties. Recently, TiO_2 nanotube arrays have attracted much attention in charging storage systems because of their capacity to offer high surface area and greatly improved electron transfer pathways compared with non-oriented structures, which favour higher charge propagation in active materials.[16,18–23] Anodic oxidation of titanium foil, extensively studied,[24–26] offers a convenient way to achieve highly ordered and suitably back-connected titania nanotube layers on the substrate, so that the combination can be used directly as a binder-free supercapacitor electrode. The highly ordered material structure offers the advantages of (i) more direct transport pathways uninterrupted by interparticle connections and (ii) the possibility to form surface electrical fields, which should reduce recombination by confining the injected electrons to the central zone of the tubes.[18]

In terms of charging mechanism, it has been mostly suggested that TiO_2 only contributes a very low non-faradic capacitance and almost no faradic capacitance.[27–29] In general, titania capacitors would resemble conventional electric double layer capacitors, which act by a non-faradic mechanism with a very low specific capacitance of 10–40 μF cm^{-2} in the charge–discharge process. It is widely believed that bare titania, due to high electric resistance and low specific surface area, shows low electrochemical capacitance. However, it has been reported that decreasing the particle size of TiO_2 to less than 10 nm results in pseudocapacitive behaviour of the resultant material, allowing for an increase in the capacitance of anatase of up to 90–120 μF cm^{-2}.[6,30]

There are many approaches which can lead the way to overcome electrical resistivity, such as electrochemical[18,31] and thermal treatments.[18,19] Changes in electrical properties can also be attributed to changes in crystallinity.[16,17,19] To the best of the authors' knowledge, highly ordered three-dimensional networks of TiO_2 nanotubes have only been used as a support to fabricate composite electrodes for electrochemical capacitor applications.[16,22] The properties of metal oxides at nanoscale, especially TiO_2, are very sensitive to oxygen content in the lattice and the related non-stoichiometry. So far, little is known about the effects of oxygen non-stoichiometry on capacitance properties. The properties of non-stoichiometric oxides are more strongly affected by their defect disorder rather than by their structure.

Institute for Superconducting and Electronic Materials, ARC Centre for Electromaterials Science, University of Wollongong, Wollongong, NSW, 2519, Australia. E-mail: ms591@uowmail.edu.au; Fax: +61 (2)42215731; Tel: +61 (2) 42981470

The most common procedure applied in the modification of non-stoichiometry and its related properties involve doping with cations and anions, among which oxygen is an important dopant for metal oxides.[32,33]

This paper presents the effects of different heat-treatment routes on capacitance, crystallinity, oxygen deficiency, and the electrical properties of titania nanotubes prepared by anodic oxidation.

Experimental procedures

The anodization was conducted on Ti foil (99.7% purity, Sigma) acting as the anode, with platinum foil as the cathode. The electrolyte consisted of 0.2 wt% NH_4F dissolved in a mixture of glycerol and de-ionized water (9 : 1 in volume). The anodization was performed under a constant voltage of 15 V for 17 h. After being dried in air, nanotubes were subjected to different heat-treatment regimes. Two samples were heated at 580 °C for 1 h in air and under argon atmosphere and labelled as sample I (one-step annealing/air) and sample II (one-step annealing/Ar), respectively. Two more samples were prepared under the same conditions, but the preparation was followed by heating up to 630 °C for 1 more hour under argon atmosphere. These samples were labelled as sample III (two-step annealing/air–Ar) and sample IV (two-step annealing/Ar–Ar).

To investigate the surface morphology and microstructure of the TiO_2 nanotubes, field emission scanning electron microscopy (FE-SEM; JEOL JSM-7500FA), X-ray diffraction (XRD; GBC MMA X-ray diffractometer with Cu-K_α radiation), and Raman spectroscopy (LabRAM HR, Horiba Jobin Yvon SAS) were employed.

A conventional cell with a three-electrode configuration was used for electrochemical characterization. The aligned titania nanotubes grown on the surface of the Ti substrate were used directly as the working electrode. A platinum sheet and an Ag/AgCl (KCl saturated) electrode were used as the counter and reference electrodes, respectively. Electrochemical measurements were performed in 1 M KCl aqueous solution. Cyclic voltammetry (CV) and electrochemical impedance spectroscopy (EIS) measurements were carried out by an electrochemical workstation (CHI660B, CH Instruments, Inc.). CV tests were conducted over a voltage range of −0.2 to 0.6 V at various scan rates (from 1 to 100 mV s^{-1}). EIS measurements were performed between 100 kHz and 1 Hz under a constant potential of −0.1 V using a 5 mV rms sinusoidal modulation. Galvanostatic charge–discharge (CD) testing was applied using a battery system (LAND CT2001A) to investigate the cycle life of the electrode.

Results and discussion

Fig. 1 shows typical FE-SEM micrographs of the TiO_2 nanotubes. The average inner diameter, wall thickness, and length of the as-grown TiO_2 nanotubes measured from FE-SEM images are approximately 30–60 nm, 10–20 nm, and 900–1000 nm, respectively. The nanotubes tend to shrink after post-annealing, however, the structure of nanotubes is still intact. Fig. 1 shows that the TiO_2 nanotubes are ordered and vertically aligned, and that a large surface area on the Ti substrate has been successfully covered by them. The ripples observed along the outer walls of the tubes are prone to happen in low viscosity electrolytes containing glycerol, which is a less aggressive electrolyte.[16,34] The obtained compact, gap-free thin sheet of nanotubes can potentially act simultaneously as both an active material and a current collector. Also, this kind of compact gap-free material has the advantage of supplying pathways for electrolyte and therefore maximizing the interface and consequently, the efficiency of the active material.

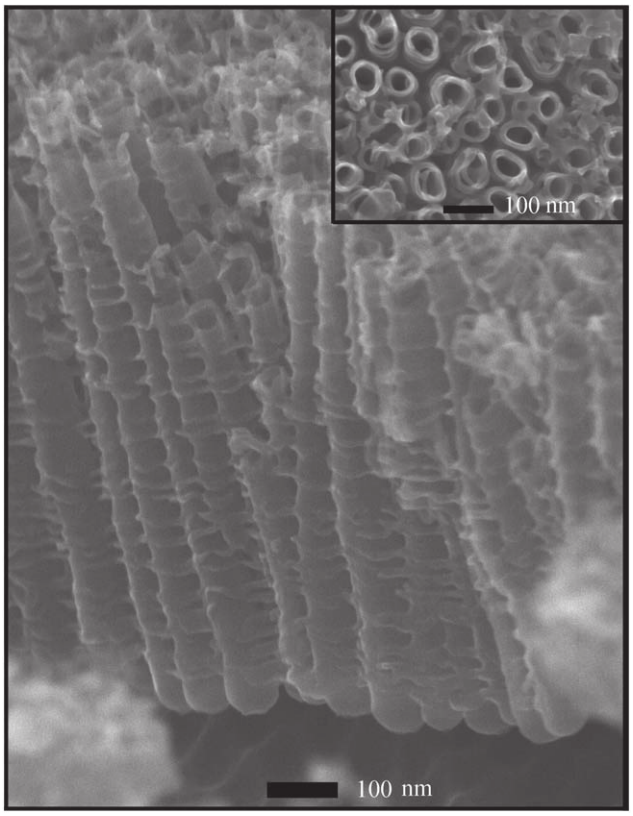

Fig. 1 Typical side view and top view (inset) FE-SEM images of as-prepared TiO_2 nanotubes.

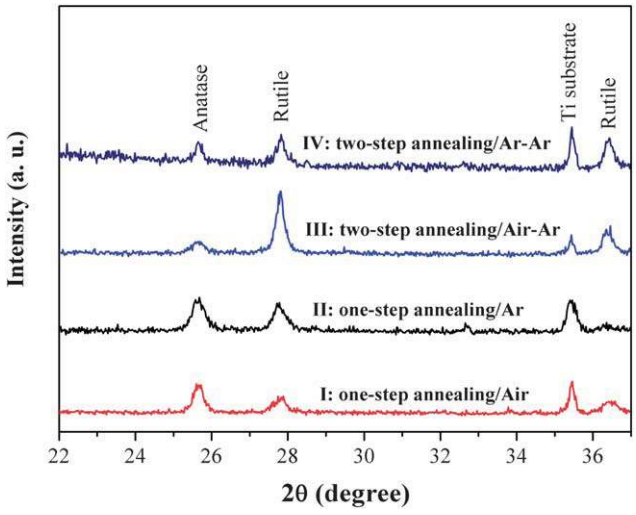

Fig. 2 XRD patterns of TiO_2 nanotubes annealed under different heating regimes.

Fig. 2 shows the XRD patterns of the samples prepared *via* one-step annealing and two-step annealing under different atmospheres. In order to eliminate the effect of the substrate contribution to the XRD pattern, XRD was only conducted in the range of 2θ from 22° to 37°. The XRD patterns obtained from the samples clearly demonstrate that one-step annealing under argon atmosphere (II) promotes the formation of rutile, in comparison to annealing under air atmosphere (I). Therefore, annealing in a neutral oxygen free environment furthers the transformation from the anatase to the rutile phase structure. It is well established that annealing in a reductive environment is likely to result in partial reduction of Ti^{4+} cations to lower valence Ti^{3+} ions.[19] At the same time, defects, such as oxygen vacancies, can be generated in the TiO_2 structure due to partial oxygen loss.[19] Furthermore, the kinetics of the phase transformation from anatase to rutile (A → R) is well studied by different researchers.[35–37] It is well understood that in the A → R transformation, the Ti–O bonds of the anatase phase structure break and are rearranged to form rutile. Oxygen vacancies overcome the activation energy of this transformation and accelerate it.[35,36]

A comparison between sample II and sample IV demonstrates that even one hour of further annealing at higher temperature in the same environment resulted in promotion of the phase transformation. The same trend was observed in samples annealed in air, both alone (I) and with subsequent annealing at higher temperature under Ar atmosphere (III). The reasons are: first, higher temperature improves the A → R phase transformation[38] and second, as was mentioned above, annealing under an inert atmosphere will result in more rutile phase due to oxygen depletion.

The thermal stability of anodized titania nanotubes and related phase changes due to annealing under different conditions were fully investigated by Raman spectroscopy (Fig. 3(a)). The Raman bands located at ~142 cm^{-1}, ~194 cm^{-1}, ~394 cm^{-1}, ~513 cm^{-1}, and ~634 cm^{-1} are attributed to anatase phase, and the bands located at ~141 cm^{-1}, ~237 cm^{-1}, ~447 cm^{-1}, and ~610 cm^{-1} are assigned to rutile phase.[36,39] The Raman spectra serve as a further proof that increasing the temperature induces the transition from anatase to rutile phase. Furthermore, in a tetragonal system, where there is out-of-phase motion of oxygen atoms along the *c*-axis, the E_g mode is much more sensitive to oxygen deficiencies than the Ti–O stretching mode. Therefore, the change in the E_g mode can serve as direct evidence of oxygen vacancies. The effect can also show itself in much broader Raman bands, which are typically due to long-range Coulomb interactions of Ti atoms and basal oxygen atoms. However, the observed line broadening in the case of anatase phase can be explained by the phonon confinement phenomenon which typically occurs when the crystallite size is less than ~20 nm. Thus, the asymmetrical broadening and the gradual shift of the anatase Raman peaks can be attributed to the phonons in the Brillouin zone which contribute to the first order Raman spectra. On the contrary, the broadening and the downshift of rutile Raman peaks most likely arise from oxygen deficiency, which effectively determines the Raman lineshapes.[40,41] Peak broadening, full width at half maximum (FWHM), and downshift of the rutile Raman band located at 447 cm^{-1} are illustrated in Fig. 3(b) and (c). These results confirm

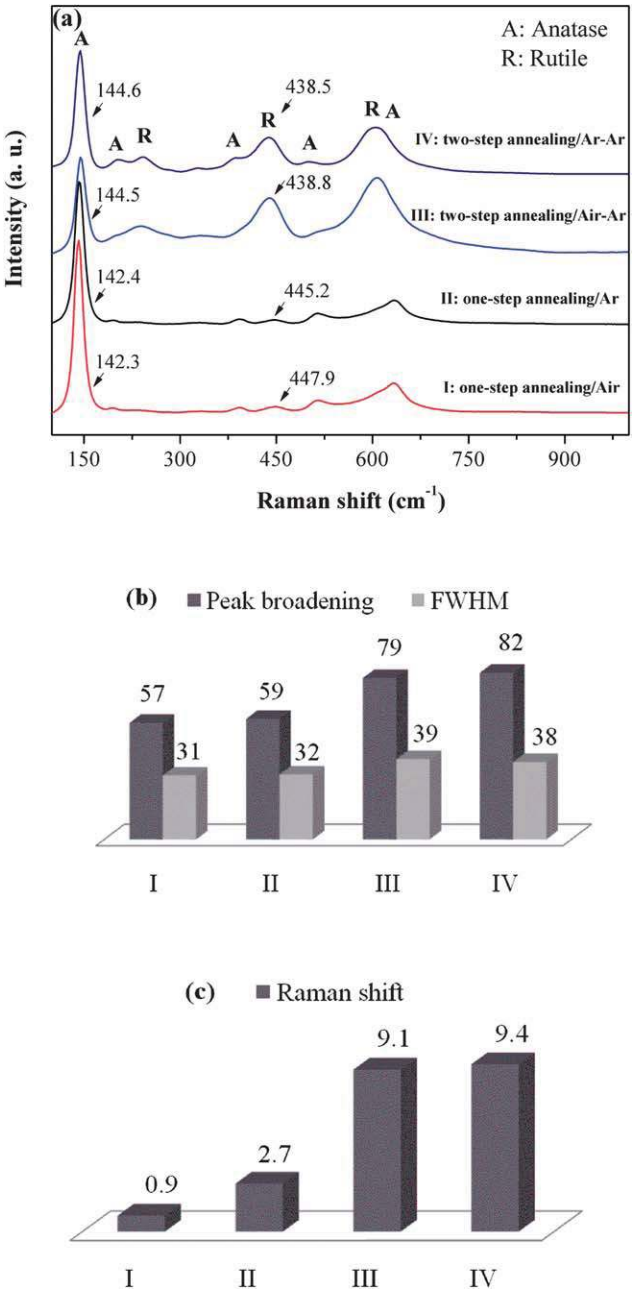

Fig. 3 (a) Raman spectra of TiO_2 nanotubes annealed under different heating regimes; (b) peak broadening and FWHM of rutile Raman band located at 447 cm^{-1}, and (c) Raman shift of rutile Raman band located at 447 cm^{-1}.

that the final structures of the sample annealed in argon for 2 hours (IV) and the sample annealed in air and then argon (III) exhibit many more oxygen deficiencies than that of the sample that was only annealed under argon atmosphere for 1 hour (II). Briefly, as oxygen becomes depleted in the anatase phase in an atmosphere with a very low partial pressure of oxygen, the rate of anatase to rutile transformation can be greatly increased, resulting in an anatase to rutile phase transformation, a process that normally requires temperatures in excess of 700 °C. Oxygen depletion results in the spatial disturbance of the oxygen framework, which, in turn, results in the breakage of a number of

Ti–O bonds and the rearrangement of the anatase pseudo-close-packed planes of oxygen {112} to the rutile close-packed planes {100}.[35] The main change induced by oxygen depletion is the strong enhancement, change of position, and broadening of the main rutile peak. Further oxygen depletion of the structure, for the samples heat-treated at 630 °C for two hours in air and argon (III) or only argon atmosphere (IV), makes the rutile band broader and causes a shift to 438 cm^{-1}, as seen in Fig. 3(a).

The electrochemical properties of the titania nanotubes annealed under different conditions were studied by CV, CD, and EIS techniques. The CV responses of the samples at a scan rate of 100 mV s^{-1} are shown in Fig. 4(a)–(c). Cyclic voltammetry tests were carried out at potentials between −0.2 and 0.6 V using 1 M KCl aqueous electrolyte solution. An almost rectangular shaped curve, as expected from an ideal capacitor,[42] was observed in the case of samples heat-treated under Ar atmosphere. The areas under the curves demonstrate a significant increase in capacitance over what has been reported in the literature and thus indicate the enhancement of the specific capacitance for these types of electrodes. However, the insignificant area under the rectangular curve for the sample merely annealed in air atmosphere (I) reflects its low capacitance compared to the samples exposed to Ar (II, III, and IV). The specific capacitance (C_s) of the electrodes was calculated from eqn (1):

$$C_s = C/S = I/[(dV/dt) \times S] \quad (1)$$

where I is the charge–discharge current, dV/dt is the scan rate, and S is the surface area of the working electrode. The specific capacitance of samples I, II, III, and IV at a scan rate of 1 mV s^{-1} is 30, 521, 294, and 911 μF cm^{-2}, respectively. According to the obtained results, the specific capacitance values of TiO_2 nanotubes heat-treated under argon atmosphere are one to two orders of magnitude higher than the values reported for titania and conventional electric double layer supercapacitors. However, the change in terms of capacitance was just marginal in the sample heat-treated under air atmosphere.

It is well-known that high conductivity of the active materials will enhance capacitance properties.[18] The higher conductivity can be further investigated in terms of geometrical aspects, reduction conditions, and phase structures. Highly ordered nanotube arrays can be viewed as nanostructures with direct pathways for electron transfer, which greatly reduces the disturbance from interparticle connections, offering the possibility that the initially low conductivity of titania structures can be overcome. Moreover, as proposed in the literature, these channels, as a form of open porosity, facilitate the ionic mass transfer through mesopores by providing pathways through which the dynamic sheath of solvent molecules, the solvation shell, can easily pass. The higher ionic mass transfer consequently results in higher capacitance values. Moreover, changing the electrical properties of oxides through changing the reduction conditions is an already well-established technique in the literature, *i.e.* annealing TiO_2 in an inert atmosphere to provide higher conductivity due to the conversion of Ti^{4+} to Ti^{3+}.[19,25,31] The electrical conductivity of TiO_{2-x} is proportional to the oxygen vacancies, which depend on the ambient oxygen pressure.[43] Furthermore, TiO_2 is an intrinsic n-type semiconductor with a band gap of approximately 3.2 eV (for anatase phase) and 3.1 eV (for rutile phase). However, in the reduced state, the higher density of Ti^{3+} leads to a decrease in the band gap to an approximate value of 2.4 eV.[31] The electrochemical and electrical properties can be also attributed to the crystallinity.[19] It seems

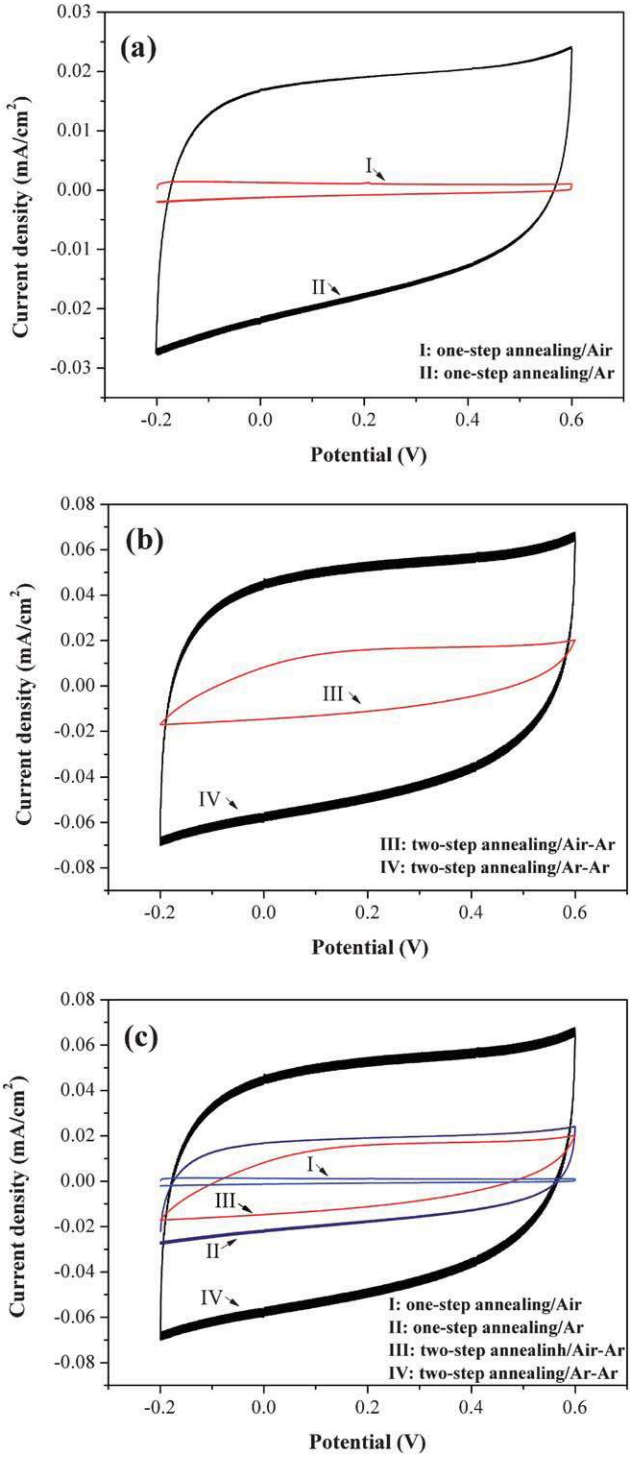

Fig. 4 Overlaid CV curves of (a) sample I: one-step annealing/air and II: one-step annealing/Ar, (b) sample III: two-step annealing/air–Ar and IV: two-step annealing/Ar–Ar, and (c) all samples, in 1 M KCl at a scan rate of 100 mV s^{-1}.

that two-step annealing under Ar atmosphere (IV) consequently results in TiO_2 nanotubes with higher conductivity.

Fig. 5(a) presents the galvanostatic CD curves of TiO_2 nanotubes subjected to two-step annealing under Ar atmosphere (IV) at different current densities. There is an almost linear relationship between voltage and charging–discharging time at higher current densities, which is expected from non-faradic electron double layer capacitors.[44] Nevertheless, at low current density, a slightly non-linear curve can be observed, which typically indicates a reaction in the charging process. Based on the literature, TiO_2 only contributes a very low non-faradic capacitance and almost no faradic capacitance.[27–29] Additionally, when the active material is in the fully oxidized state, there is no pseudocapacitive contribution.[28] Although we observed no evidence of any faradic reactions in the charge–discharge process based on the CV curves, the CD tests showed a reaction in the charging step. Therefore, it is safe to assume that the oxygen depletion derived from annealing in the reductive atmosphere resulted in an increase in the capacitance due to a faradic reaction.

The specific capacitance of the sample IV (two-step annealing/Ar–Ar) at a current density of 10 μA cm^{-2} is presented as a function of cycle number in Fig. 5(b). From the experimental data, even after 500 cycles, fairly stable capacitance is maintained, and no change in charge–discharge can be observed. At the end of five hundred cycles, the nanotube electrode maintains a symmetric charge–discharge shape with approximately 98% capacitance retention. The first 10 and last 10 cycles are also shown as insets in Fig. 5(b).

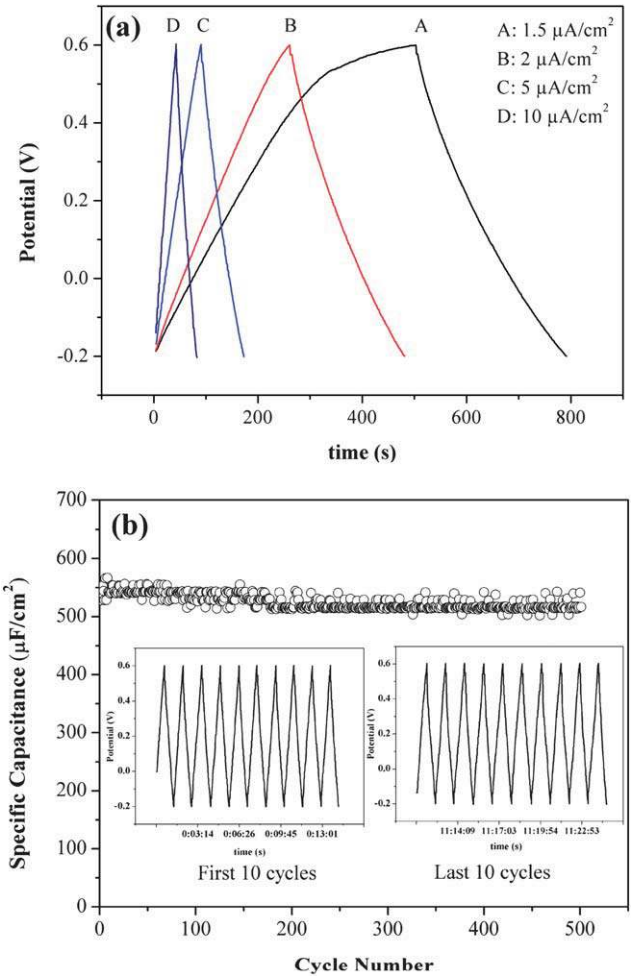

Fig. 5 (a) Galvanostatic charge–discharge plots of IV: two-step annealing/Ar–Ar; (b) specific capacitance of IV calculated from charge–discharge test *versus* cycle number along with first 10 and last 10 charge and discharge cycles as insets at a current density of 10 μA cm^{-2}.

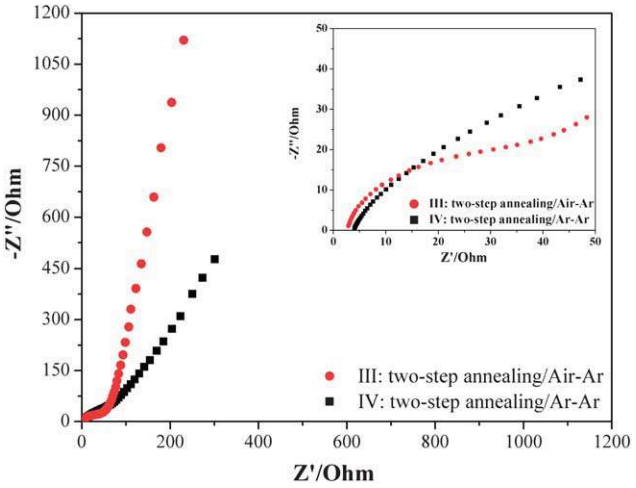

Fig. 6 Nyquist plots of sample III: two-step annealing/air–Ar and IV: two-step annealing/Ar–Ar, with the inset showing an enlargement of the high frequency region.

Fig. 6 compares the Nyquist plots of sample III and sample IV, with EIS carried out in a frequency range of 1 Hz to 100 kHz at a constant potential of −0.1 V and an AC voltage amplitude of 5 mV. The high frequency regions of the spectra are shown as the inset. A semicircular arc was observed in the sample treated in air and then under argon atmosphere (III), indicating a charge transfer limiting process, which is usually the result of a parallel combination of internal resistance and capacitance. However, no such semicircular arc was observed for the sample annealed only in pure argon (IV), which corresponds to good charge transfer of the working electrode and indicates that there is no electrical resistance. The slope in both samples increases at low frequency, which represents the diffusion of ions in the structure of the electrode and indicates pure capacitive behaviour. The slope of the curve is a result of the frequency dependence of ionic diffusion in the electrolyte to the electrode interface. These remarkable results demonstrate that the fabrication of samples with a particular heating regime results in high electrical conductivity of TiO_2 and therefore high charge propagation in TiO_2.

Conclusions

A new approach for the fabrication of high capacitance titania nanotubes is introduced. Peak broadening, FWHM and downshift of rutile Raman bands confirmed the existence of oxygen vacancies inside TiO_2 nanotubes prepared by an anodic oxidation method and subsequent annealing in argon atmosphere. Such oxygen vacancies overcome the activation energy of the breakage and rearrangement of Ti–O bonds and accelerate the transformation of A → R. Such a non-stoichiometric structure could enhance the capacitance of titania by one to two orders of

magnitude compared with the values reported for conventional titania and conventional electric double layer supercapacitors. Based on cyclic voltammetry results, no evidence of any faradic reactions was observed in working electrodes, however, the charge–discharge curves showed a reaction in charging step which might be due to partial reduction of Ti^{4+} to Ti^{3+}. These findings confirmed that the oxygen depletion derived from annealing in the reductive atmosphere resulted in an increase in the capacitance due to a faradic reaction. Electrochemical impedance spectroscopy results also demonstrated that partial oxygen depleted titania structure is more conductive in charging process. Good chemical stability was confirmed by long cycling galvanostatic charge–discharge tests.

As a whole, this work introduces a novel yet simple approach to overcome high electrical resistivity of bare titania to meet the requirements of higher specific capacitance applications.

Acknowledgements

Financial support from the University of Wollongong and the Australian Research Council (ARC, grant no. DP1093952) is gratefully acknowledged. The authors would like to thank Dr Tania Silver for critical reading of the manuscript, and S. Hamed Aboutalebi and Alfred T. Chidembo for valuable discussions.

References

1 P. Simon and Y. Gogotsi, *Nat. Mater.*, 2008, **7**, 845–854.
2 Y.-F. Ke, D.-S. Tsai and Y.-S. Huang, *J. Mater. Chem.*, 2005, **15**, 2122–2127.
3 M. S. Halper and J. C. Ellenbogen, *Supercapacitors: a Brief Overview*, MITRE Nanosystems Group, Virginia, 2006.
4 D. Pech, M. Brunet, H. Durou, P. Huang, V. Mochalin, Y. Gogotsi, P.-L. Taberna and P. Simon, *Nat. Nanotechnol.*, 2010, **5**, 651–654.
5 S. Vivekchand, C. Rout, K. Subrahmanyam, A. Govindaraj and C. Rao, *J. Chem. Sci.*, 2008, **120**, 9–13.
6 C.-M. Chuang, C.-W. Huang, H. Teng and J.-M. Ting, *J. Electrochem. Soc.*, 2010, **157**, K113–K117.
7 J. R. Jennings, A. Ghicov, L. M. Peter, P. Schmuki and A. B. Walker, *J. Am. Chem. Soc.*, 2008, **130**, 13364–13372.
8 T. Stergiopoulos, A. Ghicov, V. Likodimos, D. S. Tsoukleris, J. Kunze, P. Schmuki and P. Falaras, *Nanotechnology*, 2008, **19**, 235602.
9 G. K. Mor, O. K. Varghese, C. A. Grimes, M. A. Carvalho and M. V. Pishko, *J. Mater. Res.*, 2004, **19**, 628–634.
10 S. K. Mohapatra, K. S. Raja, V. K. Mahajan and M. Misra, *J. Phys. Chem. C*, 2008, **112**, 11007–11012.
11 J. M. Macak, F. Schmidt-Stein and P. Schmuki, *Electrochem. Commun.*, 2007, **9**, 1783–1787.
12 V. A. Alves, L. A. da Silva and J. F. C. Boodts, *Electrochim. Acta*, 1998, **44**, 1525–1534.
13 G. Bo, Z. Xiaogang, Y. Changzhou, L. Juan and Y. Long, *Electrochim. Acta*, 2006, **52**, 1028–1032.
14 K.-H. Chang and C.-C. Hu, *Electrochim. Acta*, 2006, **52**, 1749–1757.
15 F. Fabregat-Santiago, H. Randriamahazaka, A. Zaban, J. Garcia-Canadas, G. Garcia-Belmontea and J. Bisquerta, *Phys. Chem. Chem. Phys.*, 2006, **8**, 1827–1833.
16 H.-T. Fang, M. Liu, D. W. Wang, T. Sun, D. S. Guan, F. Li, J. Zhou, T. K. Sham and H. M. Cheng, *Nanotechnology*, 2009, **20**, 225701.
17 D. Dambournet, I. Belharouak and K. Amine, *Chem. Mater.*, 2010, **22**, 1173–1179.
18 F. Fabregat-Santiago, E. M. Barea, J. Bisquert, G. K. Mor, K. Shankar and C. A. Grimes, *J. Am. Chem. Soc.*, 2008, **130**, 11312–11316.
19 P. Xiao, D. Liu, B. B. Garcia, S. Sepehri, Y. Zhang and G. Cao, *Sens. Actuators, B*, 2008, **134**, 367–372.
20 D. Regonini, C. R. Bowen, R. Stevens, D. Allsopp and A. Jaroenworaluck, *Phys. Status Solidi A*, 2007, **204**, 1814–1819.
21 V. Zwilling, M. Aucouturier and E. Darque-Ceretti, *Electrochim. Acta*, 1999, **45**, 921–929.
22 N. K. Shrestha, Y.-C. Nah, H. Tsuchiya and P. Schmuki, *Chem. Commun.*, 2009, 2008–2010.
23 Y. Xie and D. Fu, *Mater. Res. Bull.*, 2010, **45**, 628–635.
24 W. Wei, S. Berger, C. Hauser, K. Meyer, M. Yang and P. Schmuki, *Electrochem. Commun.*, 2010, **12**, 1184–1186.
25 J. M. Macak, C. Zollfrank, B. J. Rodriguez, H. Tsuchiya, M. Alexe, P. Greil and P. Schmuki, *Adv. Mater.*, 2009, **21**, 3121–3125.
26 J. M. Macak, M. Zlamal, J. Krysa and P. Schmuki, *Small*, 2007, **3**, 300–304.
27 Y. Xie, L. Zhou, C. Huang, H. Huang and J. Lu, *Electrochim. Acta*, 2008, **53**, 3643–3649.
28 T. Brezesinski, J. Wang, S. Tolbert and B. Dunn, *J. Sol-Gel Sci. Technol.*, 2010, DOI: 10.1007/s10971-010-2183-z.
29 B. E. Conway and W. G. Pell, *J. Solid State Electrochem.*, 2003, **7**, 637–644.
30 J. Wang, J. Polleux, J. Lim and B. Dunn, *J. Phys. Chem. C*, 2007, **111**, 14925–14931.
31 J. M. Macak, B. G. Gong, M. Hueppe and P. Schmuki, *Adv. Mater.*, 2007, **19**, 3027–3031.
32 J. Nowotny, *Energy Environ. Sci.*, 2008, **1**, 565–572.
33 J. Nowotny, T. Bak and T. Burg, *Phys. Status Solidi B*, 2007, **244**, 2037–2054.
34 J. M. Macak, H. Tsuchiya, L. Taveira, S. Aldabergerova and P. Schmuki, *Angew. Chem., Int. Ed.*, 2005, **44**, 7463–7465.
35 R. D. Shannon and J. A. Pask, *J. Am. Ceram. Soc.*, 1965, **48**, 391–398.
36 X. Pan and X. Ma, *J. Solid State Chem.*, 2004, **177**, 4098–4103.
37 H. Zhang and J. F. Banfield, *J. Mater. Chem.*, 1998, **8**, 2073–2076.
38 M. Salari, S. M. M. khoie, P. Marashi and M. Rezaee, *J. Alloys Compd.*, 2009, **469**, 386–390.
39 A. Golubović, M. Šćepanović, A. Kremenović, S. Aškrabić, V. Berec, Z. Dohčević-Mitrović and Z. Popović, *J. Sol-Gel Sci. Technol.*, 2009, **49**, 311–319.
40 D. Bersani, P. P. Lottici, T. Lopez and X.-Z. Ding, *J. Sol-Gel Sci. Technol.*, 1998, **13**, 849–853.
41 S. Hong, H. Cheong and G. Park, *Phys. C*, 2010, **470**, 383–390.
42 A. L. M. Reddy and S. Ramaprabhu, *J. Phys. Chem. C*, 2007, **111**, 7727–7734.
43 S. Murugesan, P. Kuppusami, N. Parvathavarthini and E. Mohandas, *Surf. Coat. Technol.*, 2007, **201**, 7713–7719.
44 H. KuanXin, Z. Xiaogang and L. Juan, *Electrochim. Acta*, 2006, **51**, 1289–1292.